

BodySense: An Expandable and Wearable-Sized Wireless Evaluation Platform for Human Body Communication

Lukas Schulthess, Philipp Mayer, Christian Vogt, Luca Benini, Michele Magno

Dept. of Information Technology and Electrical Engineering, ETH Zürich, Switzerland

Abstract—Wearable, wirelessly connected sensors have become a common part of daily life and have the potential to play a pivotal role in shaping the future of personalized healthcare. A key challenge in this evolution is designing long-lasting and unobtrusive devices. These design requirements inherently demand smaller batteries, inevitably increasing the need for energy-sensitive wireless communication interfaces. Capacitive Human Body Communication (HBC) is a promising, power-efficient alternative to traditional RF-based communication, enabling point-to-multipoint data and energy exchange. However, as this concept relies on capacitive coupling to the surrounding area, it is naturally influenced by uncontrollable environmental factors, making testing with classical setups particularly challenging.

This work presents a customizable, wearable-sized, wireless evaluation platform for capacitive HBC, designed to enable realistic evaluation of wearable-to-wearable applications. Comparative measurements of channel gains were conducted using classical grid-connected- and wireless Data Acquisition (DAQ) across various transmission distances within the frequency range of 4 MHz to 64 MHz and revealed an average overestimation of 18.15 dB over all investigated distances in the classical setup.

Index Terms—Human body communication (HBC), capacitive HBC, wireless data acquisition, energy-efficient communication, body sensor networks

I. INTRODUCTION

Wearable, intelligent, and unobtrusive sensor nodes monitoring the human body and its environment have attracted significant attention from researchers and industry [1], [2]. These devices, equipped with wireless interfaces and an increasing number of sensors, are already a commercial reality for sports & fitness, with expanding capabilities aimed at collecting valuable data for human-centric healthcare [3]. Advances in system-on-chip integration and flexible electronics have enhanced sensor integration on dynamic, non-planar surfaces like the human body, enabling localized physiological signal acquisition and processing [4]–[6]. However, distributing multiple sensors on body locations with beneficial sensing characteristics inevitably increases the stress on the communication interface due to growing synchronization and connection overhead [7], [8].

Today’s wearable devices rely predominantly on Radio Frequency (RF) wireless transmission, already one of the most expensive subsystems, consuming significant power and limiting device lifetime and usability [9], [10]. Due to its widespread adoption and interoperability, Bluetooth Low Energy (BLE)

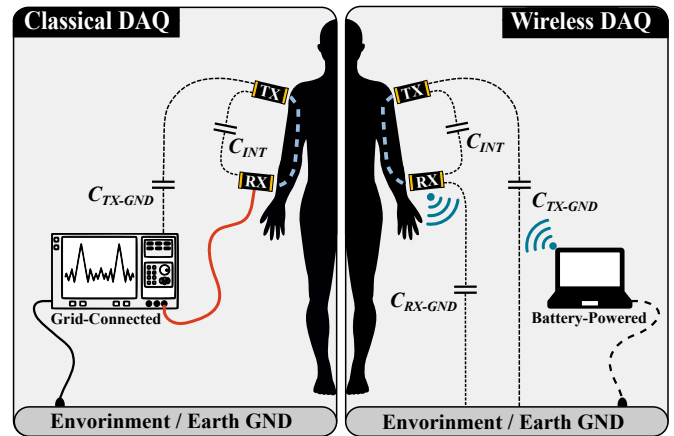


Fig. 1. Comparison between HBC DAQ setups: (left) Classical DAQ setup using grid-powered measurement tools, (right) Miniaturized and fully-wireless DAQ setup.

has emerged as the de facto standard for wearable communications. However, BLE, like other low-power wireless RF transmission technologies, may not be the optimal choice for all wearable applications. It faces challenges such as relatively high power consumption and vulnerability to security risks [11].

These limitations can make BLE less suited for ensuring consistently reliable, energy-efficient, and pervasive operation in wearables. To reduce the impact of the communication interface on the energy budget, RF devices can be periodically deactivated, a method known as duty cycling. However, while duty cycling can be effective, it inevitably introduces latency and does not eliminate power consumption during idle listening. An alternative approach is the design of always-on wireless receivers that have the ability to detect wireless messages of interest while consuming power in the micro to nano-watt range [12], [13]. However, these solutions fail to enable battery-free and, thus, truly pervasive operation. A paradigm shift in communication and power management is essential to realize the vision of a Wireless Body Area Network (WBAN) with distributed, battery-free, on-body wearables.

Emerging techniques like HBC offer a promising alternative. By using the conductive properties of the human body as a communication medium, HBC can address the limitations of BLE and other RF wireless communication by significantly

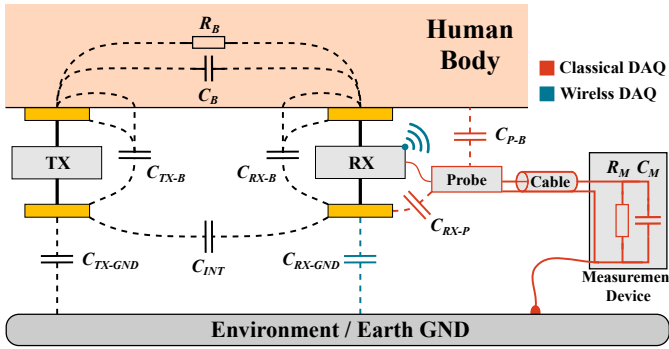


Fig. 2. Equivalent circuit for classical DAQ (red) and wireless DAQ (blue).

reducing power consumption, mitigating external interference, and enhancing security against external attacks. [14]–[16]. Unlike conventional RF transmission techniques, such as BLE, Ultra-Wideband (UWB), or Radio Frequency Identification (RFID), capacitive HBC employs the electrical conductivity of the human body to exchange information between devices [17]. Thanks to that property, capacitive HBC has the potential for secure [18], [19], body-constraint, and efficient data and energy transmission [20]–[22], making it an ideal solution for future wearable devices [16].

This work presents a wearable-sized evaluation platform for HBC. Custom-designed and compact, it enables HBC evaluations in wearable-to-wearable application scenarios by minimizing measurement errors caused by artificially strengthened return paths. Comparable in size to commercial smartwatches, the modular evaluation platform, named *BodySense*, is tailored to allow testing under realistic conditions. This platform will be used to evaluate the potential for creating energy-efficient body sensor networks. In particular, this article presents the following contributions.

- 1) The design of a versatile, expandable, wearable-sized wireless evaluation platform for HBC, enabling practical and reliable measurements.
- 2) An analysis of the channel gain across multiple transmission distances at frequencies between 4 MHz and 64 MHz, for both wearable-to-wearable and wearable-to-grid-connected application scenarios.
- 3) The demonstration of the significance of a fully wearable evaluation setup for capacitive HBC by comparing the channel gains between classical and wearable DAQ.

The rest of this article is organized as follows: Section II positions this work within the context of the state of the art. Section III details the design and implementation of the *BodySense* hardware platform. The evaluation setup topology is outlined in section IV, with the corresponding measurement results presented in section V. Finally, section VI summarizes the key findings and concludes this work.

II. BACKGROUND AND RELATED WORK

Based on the underlying coupling principle, HBC is divided into three main methods: *Capacitive coupling (CC)*, *galvanic coupling (GC)*, and *magnetic coupling (MC)*. Capacitive HBC uses a signal electrode connected to the body and a

floating ground electrode. It achieves low forward path loss throughout the body, but its performance depends on the return path and load capacitances [23], limiting its use in implantable devices [24]. *Galvanic HBC* injects differential signals using two body-attached electrodes. Signal quality predominantly depends on the electrode size, spacing, and parasitic capacitances. *Magnetic HBC* benefits from low tissue permeability, making it effective for non-Line-of-Sight (nLoS) communication and intra-body communication [25]. However, its range is limited by the magnetic near-field.

When comparing the coupling principles presented above, capacitive HBC shows the best performance when it comes to longer-distance and low-power body-centered communication [23]. The transmitter couples a signal over the skin-attached electrode to the conductive layers under the human skin, utilizing a low-impedance forward path between the transmitters and the receivers' skin electrodes [26]. The floating ground electrodes form the return path by direct capacitive coupling between each other for short distances or over the environment for longer distances. Whereas the forward path is subject to minor fluctuations caused by the coupling quality of the skin-electrode and the individual physical composition [27], the return path is heavily dependent on the environment, acting as a limiting factor for reception quality. Inter-body coupling to other people [18] or coupling to any larger conductive surface such as measurement equipment, laptop, and cables strengthens the return path, leading to over-optimistic results, see Figure 1, left. This makes it difficult to reliably quantify influences on the communication link in a controlled manner for wearable-to-wearable scenarios [28]. Hence, the analysis in a wearable-to-wearable scenario is necessary to eliminate over-estimation in amplitude and power reception of the received signal that arises from artificially enhanced ground coupling over the attached test equipment, see Figure 2.

Several recent works propose chip-integrated front-ends for capacitive HBC achieving pJ bit^{-1} communication links with data rates of up to 20 kbit s^{-1} [22], [29], demonstrating a significant reduction in energy consumption for data transfer [16]. Likewise, recent works exploit capacitive HBC for power transmission, demonstrating the possibility of transferring up to tens of μW over the whole body. Modak et al. presented a HBC Wireless Power Transfer (WPT) IC in a 65 nm process, achieving power transfer of $240 \mu\text{W}$ in a machine-to-machine configuration (close distance, perfect coupling to earth-ground) and $5 \mu\text{W}$ in a wearable-to-wearable configuration (long distance, bad coupling to earth-ground) [22].

Although these numbers are remarkable, all works clearly highlight the challenges of capacitive HBC due to the variability of electrical characteristics within and between humans and its reliance on an earth-ground coupled return path. These factors make direct comparisons between studies particularly difficult, as results are only partially reproducible [15]. Furthermore, previous research predominantly evaluates system performance using bulky, well-coupled laboratory equipment, often leading to overly optimistic outcomes. In contrast, this work focuses on designing a reliable setup capable

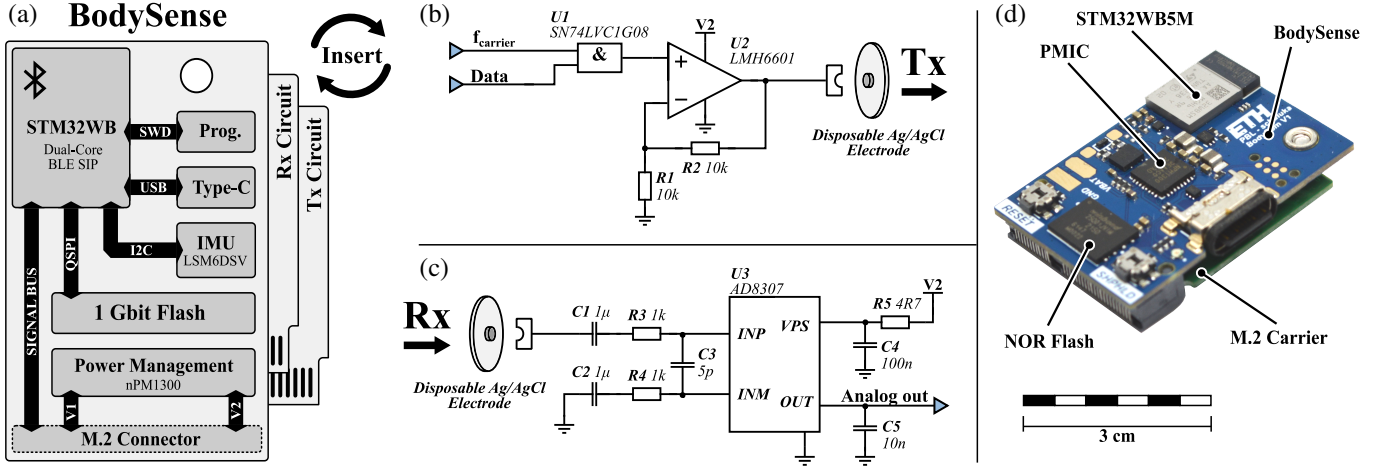


Fig. 3. System overview: (a) High-level block diagram of the main platform *BodySense*, (b) Tx carrier circuit, (c) Rx carrier circuit, (d) *BodySense* platform, equipped with M.2 carrier.

of accurately measuring HBC performance under realistic, application-oriented conditions.

III. SYSTEM DESIGN

BodySense is an expandable and wearable-sized wireless evaluation platform for human body communication that has been designed to assess HBC under realistic conditions. With an overall size of $33.5 \text{ mm} \times 22 \text{ mm}$, it is comparable to commercial smartwatches and is thus representable for wearable-to-wearable application scenarios. Figure 3 shows a simplified block diagram of the main board, detailed schematics of the designed Tx and Rx frontends, and the hardware realization.

A. System Overview

As the core platform, *BodySense* integrates essential circuits, including the computational unit and power management subsystem, and provides flexible expandability via an M.2 connector. It is built around the *STM32WB5MMG* module, an ultra-low-power, BLE-enabled System in Package (SiP) that integrates an ARM Cortex-M4 MCU running at up to 64 MHz as the primary core and an ARM Cortex-M0+ hosting the BLE stack. Additionally, the module comprises passive components for power supply stabilization, antenna matching, and clock generation. The extensive set of analog and digital peripherals, combined with its compact form factor of $11 \text{ mm} \times 7.3 \text{ mm}$ and integrated wireless connectivity, makes the module an excellent foundation for orchestrating *BodySense*.

The Power Management IC (PMIC) *nPM1300* supplies power to *BodySense* and its extension board while also monitoring the battery's state of charge and managing recharging. Two integrated software-configurable DC-DC converters power the mixed-signal circuitry. For the presented Rx and Tx circuits, these converters are configured to output $V1 = 2.7 \text{ V}$ and $V2 = 3.3 \text{ V}$, respectively. Load switches enable power gating of the extension board, thereby extending battery life. Additionally, a 1 Gbit *W25Q01JV* NOR flash provides onboard data logging capabilities.

An M.2 connector provides electrical and mechanical connectivity between *BodySense* and the carrier board, offering

a versatile interface for future circuit designs and expansion. Dedicated instances of UART, SPI, and I2C peripherals are directly routed to the M.2 connector. Additionally, Analog to Digital Converter (ADC) inputs, timer inputs, conventional GPIO pins, and wake-up pins are made available through the M.2 connector, providing flexibility for custom front-end designs and supporting a wide range of potential extensions.

B. Application-specific M.2 carrier boards:

Two carrier boards, a receiver (Rx) and a transmitter (Tx), were designed to demonstrate the versatility of the system and to evaluate capacitive HBC in realistic application scenarios. Their detailed schematics are shown in Figure 3 (b) and (c). Development-accompanying SPICE simulations, followed by verification through benchtop measurements, confirmed the correct functionality under the defined conditions. However, variances in environmental coupling as well as in the skin impedance can vary by a factor of 10 [27] and thus have a much higher impact on the measurements than the frontend's performance variation caused by component tolerances. As a consequence, testing on the human body is the only way to obtain realistic results.

Rx Circuit: Disposable Ag/AgCl electrodes are used to capture the transmitted signal from the body. A passive band-pass filter with corner frequencies $f_L = 160 \text{ Hz}$ and $f_H = 70 \text{ MHz}$ suppresses the dominant 50 Hz mains noise and other unwanted external signals from the environment that couple to the body. The subsequent logarithmic amplifier of type *AD8307*, with an operating range from DC to 500 MHz and a dynamic range of 92 dB, generates an analog output voltage proportional to the received signal level on a logarithmic scale. It is stabilized using a capacitor and then fed to the ADC on the main board for quantization. This frontend topology provides the needed high dynamic range to measure the Received Signal Strength (RSS). *Tx Circuit:* The internal Phase-locked Loop (PLL) of the *STM32WB5MMG* module is used to generate a rectangular carrier frequency f_{carrier} , ranging from 4 MHz up to 64 MHz, directly accessible on the modules GPIO. An AND gate of type *SN74LVC1G08* is used in combination with

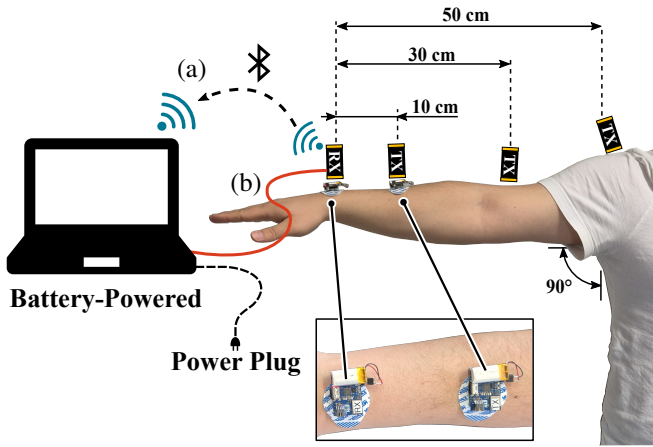


Fig. 4. Overview of the experimental setup for (a) wireless and (b) classical data readout. Transmitter and receiver placement are identical for both scenarios.

an operational amplifier of type *LMH6601*, featuring a high slew rate of $260 \text{ V}/\mu\text{s}$ and a Gain-Bandwidth Product (GBP) of 250 MHz , to generate an OOK-modulated transmit signal with a low output impedance. Finally, the signal is routed over a snap button to a disposable Ag/AgCl electrode to establish good skin contact.

IV. EXPERIMENTAL SETUP

To quantify the effect of artificially enhanced capacitive coupling for classical DAQ and compare it against wireless DAQ, three measurement series for each of the two scenarios have been conducted. One *BodySense* system has been equipped with an Rx carrier placed on the test subject's upper wrist. An adhesive Ag/AgCl wet-gel electrode from *TIGA-MED* with a diameter of 48 mm acts as skin-electrode, ensuring a low resistive contact to the body and mechanically holds the system at its position. The system ground plane and the battery act together as a floating electrode, closing the return path over the environment and earth-ground. A second *BodySense* system with a Tx carrier extension has been sequentially placed at distances of 10 cm , 30 cm , and 50 cm to the receiver, utilizing the same Ag/AgCl wet-gel electrode as skin-electrode. Figure 4 provides an overview of the transmitter and receiver positions during the experiments. Distances below 10 cm have not been investigated as the inter-device coupling significantly strengthens the return path, making it comparable to the forward path loss [19]. For each distance, a frequency sweep from 4 MHz up to 64 MHz has been performed. All measurements have been conducted in a standing position in a laboratory environment while being at least 1 m away from walls and other equipment. The arm was outstretched to the side, forming an angle of 90° between the arm and the torso's side. During the data collection, the subject stood still and kept the arm in a constant position to minimize movement-induced fluctuations in the environmental-coupled return path.

In the classical scenario, the receiver was directly connected over a USB Type-C cable, forwarding the collected data over

USB to the plugged-in computer, see Figure 4 (a). For the wireless scenario, the USB Type-C cable has been removed, and the computer has been unplugged from the grid. The data is wirelessly forwarded via BLE to the computer, as depicted in Figure 4 (b). Finally, the channel gain is calculated to measure the quality of the capacitive HBC communication channel, and the received power has been extracted to set capacitive HBC into context to conventional RF solutions.

It is essential to carefully consider the effects of signal transmission through the human body and respect its safety limits in HBC systems. The International Commission on Non-Ionizing Radiation Protection (ICNIRP) sets limits for non-ionizing radiation exposure to the human body, defining different dosimetric quantities depending on the frequency. In the frequency range between 1 Hz and 100 kHz the current density is used as limiting metric [30] and above 100 kHz the Specific Energy Absorption (SAR)-value [31]. Further, the IEEE standard C95.1-2005 defines safety levels on human exposure to RF electromagnetic fields [32]. By limiting the transmit power to maximal 5 dBm for our experiments, we ensured to meet the above-mentioned safety standards.

V. RESULTS

The measurement results for the classical as well as for the wireless DAQ scenario are discussed. In the classical scenario (Figure 5, solid lines), the lower frequencies between 4 MHz and 20 MHz , the channel gains show an almost identical frequency dependency for all distances. Whereas the more considerable distances (30 cm and 50 cm) achieve almost identical results, it shows an improvement of at least 2.6 dB for the 10 cm -distance in this frequency region. For higher frequencies above 20 MHz , the difference between 10 cm and the larger distances start to increase. Direct coupling between the transmitters and receivers floating ground electrode, illustrated as C_{INT} in Figure 2, enhances the return path for short distances. The largest channel gain with a peak value of -39.3 dB has been achieved for 38 MHz at 10 cm distance. Above 36 MHz , the 50 cm -distance shows a superior channel gain than for 30 cm , indicating an artificially improved return path caused by the wired data transmission. Overall, all three measurement series of the classical scenario are close to each other, showing a maximum difference of 8 dB at 36 MHz .

For the results of the wireless scenario (Figure 5, dashed lines), it is interesting to see that the channel gain curves show a high correlation of 0.88 between the 10 cm and 50 cm , 0.95 between 10 cm and 30 cm , and 0.98 between the 30 cm and 50 cm curves. Similar to the results of the classical scenario, the channel gain for 10 cm outperforms the more considerable distances by at least 10 dB .

Figure 6 shows the received power for both the classical and the wireless receiver scenario. The wired scenario demonstrates superior performance compared to the wireless setup across all distances, achieving a maximum power reception of -35.53 dBm at 38 MHz and a distance of 10 cm . The Rx power behaves almost constant for longer distances in the wireless scenario, achieving a minimal power reception

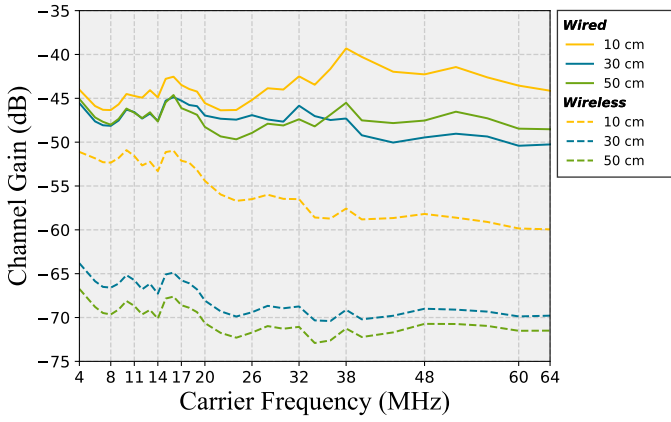


Fig. 5. Channel gains measured over different frequencies for the classical and the wireless receiver scenario.

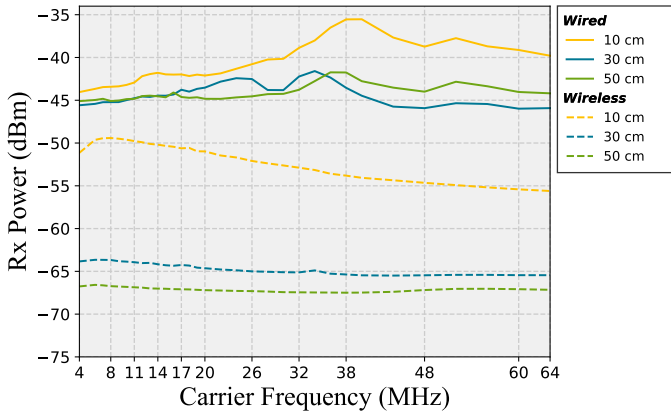


Fig. 6. Received power measured over different frequencies for the classical and the wireless receiver scenario.

−67.49 dBm with an overall fluctuation of 0.91 dB over the whole frequency range.

The experimental results visualized in Figure 5 and Figure 6 show that the classical scenario achieves a significantly higher channel gain than the wearable scenario. It is essential to recognize that the 10 cm distance outperforms the longer distances in both scenarios. Whereas the 10 cm-case is only 2.6 dB superior in the classical case, the channel gains curves for 30 cm and 50 cm lie at least 10 dB below the 10 cm-curve in the wireless setup. This is due to the strong inter-device coupling between the transmitter and receiver at close distances. In contrast to the wireless case, this effect is significantly less pronounced in the wired scenario, as all distances benefit from improved coupling. When comparing the channel gain curves for the two setups, one can readily observe that the channel gain has increased by an average of 11.17 dB for the 10 cm, 20.34 dB for 30 cm, and 22.95 dB for the 50 cm distance for the wired scenario. This proves and quantifies the significant impact of classical DAQ on measurements in the realm of capacitive HBC. The obtained channel gain for wireless DAQ shows comparable performance as described in [28]. However, a quantitative comparison of this work to the State-of-Art (SoA) remains challenging as differences in the test setup, like device size and environment, can noticeably influence the measured absolute value. Using the same test setup minimizes

the board’s effects, as capacitive coupling to the environment dominates the received signal.

To compare the communication power of capacitive HBC with BLE, the most prominent RF communication method for wearables, we define energy efficiency as a function of the data rate (energy/bit). When taking the measured Tx power of 2.71 mW at 64 MHz and assuming a reasonable data rate of 1 Mbps [33], we achieve 2.71 nJ/bit. This is comparable to Bluetooth, which achieves energy efficiencies larger than 1 nJ/bit up to 15 nJ/bit [11]. With a simple Tx frontend, capacitive HBC is able to achieve comparable energy efficiency to BLE. With a Tx power of 2.71 mW at 64 MHz, the maximal received power for distances of 10 cm, 30 cm, and 50 cm lies at −60 dBm, −69.9 dBm, and −71.9 dBm, respectively. Although these power levels are very small, they appear to converge to a fixed value at larger distances. This makes them interesting for energy harvesting applications, especially if the baseline of the received power can be increased.

VI. CONCLUSION

While conventional data acquisition setups are effective for quantifying the forward path loss, which depends on the conductive properties of the human body, they substantially alter the return path behavior by artificially modifying the capacitive coupling to earth ground. Therefore, a wireless, wearable-sized data acquisition system is essential for quantitatively evaluating the full HBC communication channel in a realistic environment with minimal measurement interference. To address this challenge, this work introduces *BodySense*, an evaluation platform for human body communication that is fully wireless, compact enough for wearable applications, and designed for extendability. To validate the proposed system, the measured channel gains of a classical, grid-connected setup and a wireless setup have been determined for distances of 10 cm, 30 cm, and 50 cm between transmitter and receiver for a frequency range between 4 MHz and 64 MHz. A comparison between the two scenarios yields an average overestimation of 18.15 dB over all investigated distances for the classical case, highlighting the importance of evaluating capacitive HBC in realistic conditions. When comparing the energy consumption of capacitive HBC with BLE, we achieved results comparable to state-of-the-art BLE frontends. This demonstrates its potential as a promising alternative to conventional RF links, offering opportunities to further enhance the overall energy efficiency of wearable devices and move closer to the realization of battery-free, body-worn sensor nodes.

ACKNOWLEDGMENT

This work was found by the Swiss National Science Foundation SNSF under the projects “BodyLink: Enabling Battery-free body-worn Sensing and Communication with Energy Transfer” (Grant Nr. 220867) and “Wearable Nano-Opto-electro-mechanic Systems” (Grant Nr. 209675).

REFERENCES

- [1] E. Svertoka, A. Rusu-Casandra, and I. Marghescu, "State-of-the-art of industrial wearables: A systematic review," in *2020 13th International Conference on Communications (COMM)*, 2020, pp. 411–415, doi: 10.1109/COMM48946.2020.9141982.
- [2] H. C. Ates *et al.*, "End-to-end design of wearable sensors," *Nature Reviews Materials*, vol. 7, p. 887–907, 2022, doi: 10.1038/s41578-022-00460-x.
- [3] C. Wu, L. Han, Y. Dong, M. Guo, R. Wang, and J. Si, "Wireless battery-free flexible sensing system for continuous wearable health monitoring," *Advanced Materials Technologies*, vol. 8, no. 10, p. 2201662, 2023, doi: 10.1002/admt.202201662.
- [4] Y. Luo *et al.*, "Technology roadmap for flexible sensors," *ACS nano*, vol. 17, 03 2023, doi: 10.1021/acsnano.2c12606.
- [5] S. W. Lee, X. Pei, J. Rajendran, and R. Esfandyarpour, "A wireless and battery-free wearable pressure sensing system for human-machine interaction and health monitoring," *IEEE Journal on Flexible Electronics*, vol. 2, no. 6, pp. 439–447, 2023, doi: 10.1109/JFLEX.2023.3300997.
- [6] J. Alcalá-Medel, D. Michaelson, R. J. Eike, and Y. Li, "Durability study of e-textile electrodes for human body communication," *Textile Research Journal*, vol. 94, no. 1-2, pp. 246–258, 2024, doi: 10.1177/00405175231197651.
- [7] A. Celik, K. N. Salama, and A. M. Eltawil, "The internet of bodies: A systematic survey on propagation characterization and channel modeling," *IEEE Internet of Things Journal*, vol. 9, no. 1, pp. 321–345, 2022, doi: 10.1109/JIOT.2021.3098028.
- [8] A. Adawy, A. Djemal, L. Wang, G. Bouattour, A. Fakhfakh, and O. Kanoun, "Design of an energy efficient sensor node for wearable applications," in *2024 IEEE International Instrumentation and Measurement Technology Conference (I2MTC)*, 2024, pp. 1–6, doi: 10.1109/I2MTC60896.2024.10560674.
- [9] K. S. Deepak and A. V. Babu, "Energy consumption analysis of modulation schemes in IEEE 802.15.6-based wireless body area networks," *EURASIP Journal on Wireless Communications and Networking*, vol. 2016, no. 1, p. 187, Aug 2016, doi: 10.1186/s13638-016-0682-5.
- [10] L. Schulthess *et al.*, "Tinybird-ml: An ultra-low power smart sensor node for bird vocalization analysis and syllable classification," in *2023 IEEE International Symposium on Circuits and Systems (ISCAS)*, 2023, pp. 1–5, doi: 10.1109/ISCAS46773.2023.10181431.
- [11] A. Datta and S. Sen, "Can wi-r enable perpetual iob nodes?" in *2023 IEEE Biomedical Circuits and Systems Conference (BioCAS)*, 2023, pp. 1–5, doi: 10.1109/BioCAS58349.2023.10388539.
- [12] R. Piyare, A. L. Murphy, C. Kiraly, P. Tosato, and D. Brunelli, "Ultra low power wake-up radios: A hardware and networking survey," *IEEE Communications Surveys & Tutorials*, vol. 19, no. 4, pp. 2117–2157, 2017, doi: 10.1109/COMST.2017.2728092.
- [13] S. Shellhammer, A. Asterjadhi, and Y. Sun, *Wake-up Radio Concept*. John Wiley & Sons, Ltd, 2023, pp. 25–42.
- [14] D. Das, S. Maity, B. Chatterjee, and S. Sen, "Enabling covert body area network using electro-quasistatic human body communication," *Scientific Reports*, vol. 9, no. 1, p. 14, 2019, doi: 10.1038/s41598-018-38303-x.
- [15] A. Datta, M. Nath, D. Yang, and S. Sen, "Advanced biophysical model to capture channel variability for eqs capacitive hbc," *IEEE Transactions on Biomedical Engineering*, vol. 68, no. 11, pp. 3435–3446, 2021, doi: 10.1109/TBME.2021.3074138.
- [16] B. Chatterjee, P. Mohseni, and S. Sen, "Bioelectronic sensor nodes for the internet of bodies," *Annual Review of Biomedical Engineering*, vol. 25, no. 1, pp. 101–129, 2023, doi: 10.1146/annurev-bioeng-110220-112448.
- [17] T. G. Zimmerman, "Personal area networks: Near-field intrabody communication," *IBM Systems Journal*, vol. 35, no. 3.4, pp. 609–617, 1996, doi: 10.1147/sj.353.0609.
- [18] M. Nath, S. Maity, S. Avlani, S. Weigand, and S. Sen, "Inter-body coupling in electro-quasistatic human body communication: theory and analysis of security and interference properties," *Scientific Reports*, vol. 11, 2020.
- [19] D. Yang, S. Maity, and S. Sen, "Physically secure wearable-wearable through-body interhuman body communication," *Frontiers in Electronics*, vol. 2, 2022, doi: 10.3389/felec.2021.807051.
- [20] R. Shukla, N. Kiran, R. Wang, J. Gummesson, and S. I. Lee, "Skinny-power: enabling batteryless wearable sensors via intra-body power transfer," in *Proceedings of the 17th Conference on Embedded Networked Sensor Systems (SenSys 2019)*, New York, NY, USA, 2019, p. 68–82, doi: 10.1145/3356250.3360034.
- [21] Y. Dong *et al.*, "Body-coupled power transceiver with node-specific body-area powering," in *ESSCIRC 2021 - IEEE 47th European Solid-State Circuits Conference (ESSCIRC)*, Grenoble, France, 2021, pp. 423–426, doi: 10.1109/ESSCIRC53450.2021.9567745.
- [22] N. Modak *et al.*, "Eqs res-hbc: A 65-nm electro-quasistatic resonant 5–240 μ w human whole-body powering and 2.19 μ w communication soc with automatic maximum resonant power tracking," *IEEE Journal of Solid-State Circuits*, vol. 57, no. 3, pp. 831–844, 2022, doi: 10.1109/JSSC.2022.3142177.
- [23] M. Nath, A. K. Ulvog, S. Weigand, and S. Sen, "Understanding the role of magnetic and magneto-quasistatic fields in human body communication," *IEEE Transactions on Biomedical Engineering*, vol. 69, no. 12, pp. 3635–3644, 2022, doi: 10.1109/TBME.2022.3174959.
- [24] v. L. Vasić, M. Cifrek, Y. Gao, and M. Du, "Preliminary characterization of capacitive intrabody communication channel under implantable-like conditions," in *2020 IEEE International Instrumentation and Measurement Technology Conference (I2MTC)*, 2020, pp. 1–5, doi: 10.1109/I2MTC43012.2020.9128564.
- [25] E. Wen, D. F. Sievenpiper, and P. P. Mercier, "Channel characterization of magnetic human body communication," *IEEE Transactions on Biomedical Engineering*, vol. 69, no. 2, pp. 569–579, 2022, doi: 10.1109/TBME.2021.3101766.
- [26] D. J. Bora and R. Dasgupta, "Estimation of skin impedance models with experimental data and a proposed model for human skin impedance," *IET Systems Biology*, vol. 14, no. 5, pp. 230–240, 2020, doi: 10.1049/iet-syb.2020.0049.
- [27] S. Maity, M. He, M. Nath, D. Das, B. Chatterjee, and S. Sen, "Bio-physical modeling, characterization, and optimization of electro-quasistatic human body communication," *IEEE Transactions on Biomedical Engineering*, vol. 66, no. 6, pp. 1791–1802, 2019, doi: 10.1109/TBME.2018.2879462.
- [28] S. Avlani, M. Nath, S. Maity, and S. Sen, "A 100khz-1ghz termination-dependent human body communication channel measurement using miniaturized wearable devices," in *2020 Design, Automation & Test in Europe Conference & Exhibition (DATE)*, 2020, pp. 650–653, doi: 10.23919/DATE48585.2020.9116556.
- [29] S. Maity, B. Chatterjee, G. Chang, and S. Sen, "Bodywire: A 6.3-pj/bit 30-mb/s -30-db sir-tolerant broadband interference-robust human body communication transceiver using time domain interference rejection," *IEEE Journal of Solid-State Circuits*, vol. 54, no. 10, pp. 2892–2906, 2019, doi: 10.1109/JSSC.2019.2932852.
- [30] I. Secretariat, "Icnirp guidelines for limiting exposure to time-varying electric and magnetic fields (1 hz – 100 khz)," *Health Physics*, vol. 99, no. 6, pp. 818–836, 2010, doi: 10.1097/HP.0b013e3181f06c86.
- [31] —, "Icnirp guidelines for limiting exposure to time-varying electric, magnetic, and electromagnetic fields (up to 300ghz)," *Health Physics*, vol. 74, no. 4, pp. 494–522, 1998.
- [32] IEEE, "Ieee standard for safety levels with respect to human exposure to radio frequency electromagnetic fields, 3 khz to 300 ghz," *IEEE Std C95.1-2005 (Revision of IEEE Std C95.1-1991)*, pp. 1–238, 2006, doi: 10.1109/IEEESTD.2006.99501.
- [33] "Wi-r technology white paper," <https://www.ixana.ai/blog/wi-r-technology-white-paper>, accessed: 2024-12-07.